

Multiple Lines of Evidence Identify U(V) as a Key Intermediate during U(VI) Reduction by *Shewanella oneidensis* MR1

Gianni F. Vettese, Katherine Morris, Louise S. Natrajan, Samuel Shaw, Tonya Vitova, Jurij Galanzew, Debbie L. Jones, and Jonathan R. Lloyd*



Cite This: *Environ. Sci. Technol.* 2020, 54, 2268–2276



Read Online

ACCESS |



Metrics & More

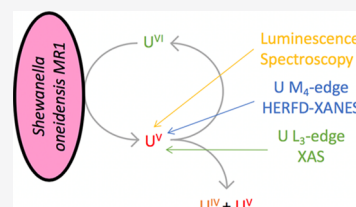


Article Recommendations



Supporting Information

ABSTRACT: As the dominant radionuclide by mass in many radioactive wastes, the control of uranium mobility in contaminated environments is of high concern. U speciation can be governed by microbial interactions, whereby metal-reducing bacteria are able to reduce soluble U(VI) to insoluble U(IV), providing a method for removal of U from contaminated groundwater. Although microbial U(VI) reduction is widely reported, the mechanism(s) for the transformation of U(VI) to relatively insoluble U(IV) phases are poorly understood. By combining a suite of analyses, including luminescence, U M₄-edge high-energy resolved fluorescence detection–X-ray absorption near-edge structure (XANES), and U L₃-edge XANES/extended X-ray absorption fine structure, we show that the microbial reduction of U(VI) by the model Fe(III)-reducing bacterium, *Shewanella oneidensis* MR1, proceeds via a single electron transfer to form a pentavalent U(V) intermediate which disproportionates to form U(VI) and U(IV). Furthermore, we have identified significant U(V) present in post reduction solid phases, implying that U(V) may be stabilized for up to 120.5 h.



INTRODUCTION

Highly soluble U(VI), as uranyl(VI), is a significant contaminant in soils and sediments associated with uranium mining, processing, and storage in nuclear sites worldwide. Reduction of mobile U(VI) to poorly soluble U(IV) can be achieved via enzymatic electron transfer mediated by anaerobic metal-reducing bacteria. This metabolism will contribute to a decrease in U mobility in the cases of “natural attenuation”, and can be further enhanced via electron donor injections, which have been proposed as a bioremediation technique for U-contaminated land and water.¹ In field-scale tests at the Rifle Field Research Site, Colorado, the potential for U(VI) removal from contaminated groundwater by indigenous Fe(III)-reducing bacteria was assessed over a 3 month period. Here, “biostimulation”, promoted by the injection of the electron donor acetate, resulted in soluble U dropping to below levels prescribed by the Environmental Protection Agency within 50 days.² Here, a marked increase in numbers of *Geobacter* species, a subsurface metal-reducing bacterium known to respire U(VI), accompanied reduction and precipitation of U(IV).^{2–5} However, subsequent re-oxidation processes lead to remobilization of the U, highlighting that the longevity of bioreduced end-points require optimization.

A series of *c*-type cytochromes traverse the outer compartments of the Gram-negative *Geobacter* cell and terminate at the surface of the outer membrane where metals, including U(VI), are reduced.⁶ In addition, conductive pili, which extend from the cell surface reportedly play a role in metal reduction.^{7,8} These reactions can also be accelerated by the addition of extracellular electron shuttles including humic acids.^{7,8}

Fluorescence spectroscopy, density functional theory, and U L₃-edge X-ray absorption spectroscopy (XAS) have all suggested that the reduction mechanism is via single electron transfer forming an intermediary uranyl(V) state which then disproportionates to more stable U(IV) and uranyl(VI) in *Geobacter sulfurreducens*.^{9–11} Furthermore, uranyl(V/VI) microparticles have been identified in a multispecies biofilm through the combined use of confocal laser scanning microscopy and fluorescence spectroscopy.¹² Other well-studied model metal-reducing bacterial species are found in the genus *Shewanella*, and here the electron transfer proteins are again well characterized. A combination of outer membrane-associated *c*-type cytochromes and extracellular electron shuttles govern U(VI) reduction.^{13–16} However, to date, no published studies have provided direct unequivocal analytical evidence of the pentavalent U(V) intermediate in the enzymatic reduction of U(VI) by *Shewanella*, or indeed any other metal-reducing bacterium.

Pu(V), as plutonyl(V), has been identified as a significant environmental species in water^{17,18} and more recently has been identified as a meta-stable intermediate in the reduction of plutonyl(VI) to form Pu(IV)O₂ nanoparticles.¹⁹ While other actinyl(V) species, specifically [Np(V)O₂]⁺ and [Pu(V)O₂]⁺, are expected to be environmentally significant,^{9,20,21} the

Received: September 2, 2019

Revised: January 6, 2020

Accepted: January 14, 2020

Published: January 14, 2020



uranyl(V) cation is relatively unstable with respect to disproportionation.²² Recent advances in ligand synthesis have permitted the isolation and characterization of several uranyl(V) compounds,^{22–30} and in aqueous media, uranyl(V) is reported as a transient species with some stabilization afforded by, for example, complexation with CO_3^{2-} species.^{31–34} While uranyl(V) triscarbonate solutions have been reported to be stable in carbonate (>0.8 M as Na_2CO_3) solutions in the pH range 10.5–12.0 for up to two weeks,^{32,33,35,36} uranyl(V) has recently been stabilized in aqueous conditions at circumneutral pH over month time-scales, via a polydentate amino-carboxylate ligand.³⁷ In the natural environment, U(V) exists in the mixed valence mineral wyartite and in the mixed oxidation state U-oxides U_3O_8 and U_4O_9 , where U(V) is incorporated in a nonuranyl-like coordination.^{38,39} Recent work also suggests that U(V) phases can show enhanced stability in the presence of iron-bearing phases typically by the incorporation of U(V) into the mineral lattice in a uranate-like coordination.^{40–48} This suggests that a single electron transfer pathway to uranyl(VI) in iron-rich environments may lead to the formation and stabilization of U(V) in the resultant iron-bearing mineral phases.

Despite its potential environmental relevance, the role of U(V) in the microbial reduction of U(VI) is still poorly understood in organisms outside the *Geobacter* genus. Even with *Geobacter* species, only a restricted number of analyses have inferred the presence of U(V); they have been conducted using extended X-ray absorption fine structure (EXAFS)⁹ and fluorescence spectroscopy.¹⁰ Here, we build on this past work to define the mechanism of U(VI) bioreduction using cultures of the model metal-reducing bacterium *Shewanella oneidensis* MR1. Through the application of luminescence spectroscopy, U M_4 -edge HERFD–XANES (high-energy resolved fluorescence detection–X-ray absorption near-edge structure, also called high-energy resolution XANES, HR–XANES^{49,50}), and U L_3 -edge XANES/EXAFS, we demonstrate unequivocally that enzymatic reduction of U(VI) by *S. oneidensis* MR1 proceeds via a U(V) intermediate state, and our study is the first to provide direct analytical evidence for U(V) via the U M_4 -edge HERFD–XANES technique. Furthermore, during a 5-day bioreduction experiment, up to 60% U(V) was identified in cell suspensions between 2.5 and 4.5 h. Interestingly, U M_4 -edge HERFD–XANES analyses identified approximately 20–30% U(V) as a persistent species at the 120.5 h bioreduction end-point, and further U L_3 -edge EXAFS analysis for this end-point sample, suggest that it was present as uranyl(V). These multitechnique observations drawing upon the state of the art U M_4 -edge HERFD–XANES analysis approach, confirm that U(V) is a key intermediate during the bioreduction of U(VI) by organisms outside the *Geobacter* genus. They also suggest that U(V) may persist as a long-lived intermediate for up to 120.5 h in addition to well characterized U(IV) bioreduction end products such as uraninite.^{51,52}

■ EXPERIMENTAL METHODS

Microbial Culture Preparation. *S. oneidensis* MR1 was obtained from the University of Manchester Geomicrobiology group culture collection. Starter cultures were grown aerobically in tryptic soy broth (Oxoid CM0876) overnight (30 °C, 100 rpm) before transfer to an anaerobic *Shewanella* minimal medium.^{14,53} The bacteria were grown to mid-exponential growth in the *Shewanella* minimal medium which contains lactate (10 mM) as the electron donor and fumarate (10 mM)

as the electron acceptor for 24 h (30 °C).^{14,53} Late log phase cultures were collected by centrifugation and washed three times in anaerobic NaHCO_3 (30 mM) buffer solution (pH 7). An aliquot of the final washed cell suspension was added to a sterile solution of 3 mM (714 ppm) U(VI) (as UO_2^{2+} in 0.001 M HCl) in NaHCO_3 (30 mM, pH 7) and was supplied with lactate (10 mM) as an electron donor. Experiments were sampled periodically over 5 days. The following samples were collected for further analysis; cell suspensions were sampled directly and included the whole reaction mixture; sub-aliquots were also centrifuged (16,160g, 5 min) and the resultant supernatant ($U_{(aq)}$) and precipitate, ($U_{(ppt)}$), samples analyzed. The total U and uranyl(VI) concentrations in the supernatant were determined by inductively coupled plasma mass–spectrometry (ICP–MS) analysis of the acidified (2% HNO_3) supernatant using an Agilent 7500CX (ICP–MS), and by luminescence spectroscopy of the frozen supernatant, respectively. Cell suspensions were measured using U L_3 -edge XAS at 2.5 and 4.5 h. At 4.5 h, we also analyzed the cell suspension and a cell pellet using U M_4 -edge HERFD–XANES. Finally, cell pellets made at 120.5 h were measured using both U L_3 -edge XAS and U M_4 -edge HERFD–XANES.

Spectroscopic Analyses. All samples were handled under anaerobic conditions throughout, and for X-ray absorption spectroscopy/luminescence spectroscopy samples were harvested and frozen immediately in liquid N_2 and stored at -80 °C under an Ar atmosphere prior to analysis. Aqueous geochemical samples were prepared at 30 min time points for luminescence spectroscopy, hourly time points for ICPMS analysis for total aqueous U, and XAS samples were prepared at approximately 2.5, 4.5, and 120.5 h.

Steady-state emission spectra were recorded on an Edinburgh Instruments FP920 phosphorescence lifetime spectrometer equipped with a finger dewar liquid N_2 cryostat, a 450 W steady state xenon lamp (with single 300 mm focal length excitation and emission monochromators in Czerny Turner configuration), and a red sensitive photomultiplier in a Peltier (air cooled) housing (Hamamatsu R928P) detector.¹⁰ Each scan was run in triplicate at -196 °C using an excitation wavelength 405 nm, and identical parameters throughout. All spectra were corrected for the excitation source and the detector response using the correction files provided in software.

U M_4 -edge HERFD–XANES measurements were performed at the ACT station of the CAT–ACT beamline at the Karlsruhe Research Accelerator (KARA), KIT lightsource.^{54,55} Again, samples were stored at -80 °C prior to analysis on the beam line and during data acquisition, samples were analyzed in a cooled cell under a $\text{He}_{(l)}$ flow. During data acquisition, beam damage was assessed by measuring several short HERFD–XANES over the white line, exposing the sample and analyzing the white line intensity in order to assess any evidence for the oxidation state drift. Throughout, we did not see any evidence for beam damage effects. The resultant U M_4 -edge HERFD–XANES spectra were normalized according to their maxima, before analysis using Athena linear combination fitting to further quantify the likely proportion of U(VI), (V), and (IV) in the samples⁵⁶ and the best results from linear combination fitting had a *R*-factor < 0.02 (Figure S5, Table S2).

U L_3 -edge XAS samples were prepared from cell suspensions and/or centrifuged solid precipitates which had been stored at -80 °C after harvesting for analysis. Samples were maintained

at $-80\text{ }^{\circ}\text{C}$ during transport to Diamond Light Source, Harwell, UK for XAS analysis on B18.⁵⁷ U L_3 -edge spectra were collected in a liquid N_2 cryostat in either fluorescence or transmission mode using a 36 element Ge detector, with in-line yttrium foil reference for energy calibration. During data acquisition, beam damage was assessed by measuring several quick EXAFS spectra, exposing the sample and analyzing the spectral features (peak height, position, and intensities) in order to assess any evidence for oxidation state drift. Throughout, we did not see any evidence for beam damage effects. Software packages ATHENA and ARTEMIS were used to analyze the EXAFS spectra⁵⁶ (Supporting Information Section S3).

RESULTS AND DISCUSSION

Aqueous Geochemistry and Luminescence Spectroscopy. When supplied with U(VI) and electron donor (lactate), washed cell suspensions of *S. oneidensis* MR1 removed up to 90% of the initial aqueous U(VI) from solution after 24 h and 99.5% after 120 h, as shown by ICPMS and luminescence spectrometry (Figure 1). The solution changed

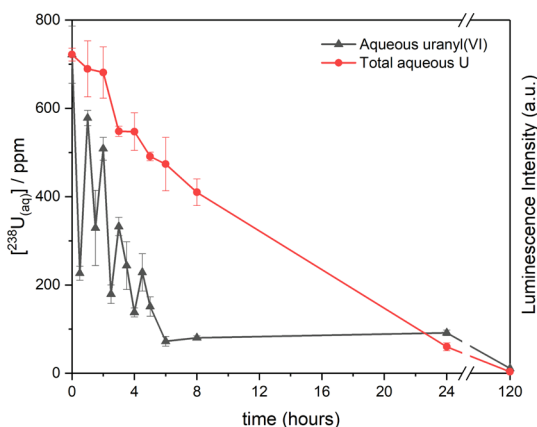


Figure 1. Aqueous uranyl(VI) (grey) and total aqueous U (red). Aqueous uranyl(VI) concentrations were determined by the luminescence intensity at $-196\text{ }^{\circ}\text{C}$ ($\lambda_{\text{ex}} = 405\text{ nm}$), and the total aqueous U concentrations were determined by ICPMS. Both measurements were recorded on the supernatant after centrifugation (16,160g, 5 min). Luminescence intensity was normalized to the initial $\text{U}_{(\text{aq})}$ concentration and the error bars represent 1 standard deviation on triplicate measurements.

from yellow to grey suggesting reduction of soluble U(VI). U sorption to autoclaved cells was quantified in a control experiment, after 2 and 4 h, 9 and 17% U was removed by adsorption to the *S. oneidensis* MR1 cells, respectively (Figure S1). Thermodynamic modeling, carried out using the PHREEQC software package, and UV-vis spectroscopy of the reaction medium suggested that under the conditions employed, uranyl(VI) triscarbonate dominates solution (Table S1, Figure S5).^{58,59} Luminescence spectroscopy of supernatant samples yielded diagnostic, vibrationally resolved U(VI), as uranyl(VI), emission spectra centered at 525 nm.¹⁰ As emission intensity is directly proportional to the uranyl(VI) concentration (provided that the uranyl(VI) speciation is unchanged), luminescence spectroscopy was used semi-quantitatively to assess the change in uranyl(VI) concentrations present in the supernatant.^{60,61} Over 24 h incubation, the luminescence emission intensity showed a decreasing

trend, but with noticeable fluctuations within the first 5 h which is consistent with a saw-tooth uranyl(VI) signal. The significant difference in concentrations of aqueous U, as determined by ICPMS, and aqueous uranyl(VI), as determined by luminescence spectroscopy, also suggests the presence of a significant fraction of nonuranyl(VI), nonluminescent (under the conditions employed) U-containing species. These results are likely due to a single electron transfer mechanism generating transient, nonluminescent (under the conditions employed) uranyl(V),⁶² followed by disproportionation to luminescent uranyl(VI) and nonluminescent (under the conditions employed) U(IV),⁶³ as observed for *Geobacter*¹⁰ (Figure 1). The fluctuations in uranyl(VI) concentrations are consistent with the previous literature suggesting a uranyl(V) intermediate proceeding via a disproportionation mechanism,^{9,10,37,41,64} and the saw-tooth pattern is not consistent with U(IV) reoxidation which generally occurs on much longer timescales (weeks–months).^{65–67}

In the current work, this implies that enzymatic reduction mediated by cells of *S. oneidensis* MR1 is occurring in a similar way to the *Geobacter* system, and via the reduction of uranyl(VI) to an intermediate U(V) species, which is not emissive in the 450–600 nm window employed following a 405 nm excitation.^{10,62} The decrease and subsequent increase in the uranyl(VI) signal steps are consistent with dynamic uranyl(V) disproportionation to luminescent uranyl(VI) and nonluminescent U(IV) species (Figures 1 and S4) and the relevant literature.^{9,10} The clear fluctuations and difference in total U versus uranyl(VI) assessed using luminescence intensity were broadly reproducible over the first 120 h of bioreduction and the kinetics are discussed in the Supporting Information (Figure S4).

X-ray Absorption Spectroscopy: U M_4 -Edge HERFD–XANES. U M_4 -edge analysis has recently been shown to be highly diagnostic for U(VI), U(V), and U(IV) species in complex systems.^{38,40,44,68} Here, U M_4 -edge HERFD–XANES data were collected at 4.5 h (on the cell suspension and cell pellet) and 120.5 h (cell pellet) to further explore the U-oxidation state distribution in the bioreduction experiment. For the 4.5 h cell pellet and cell suspension samples, the U M_4 -edge HERFD–XANES spectra were intermediate between the U(VI) and U(IV) standards (Table S2, Figure S6). We first performed a linear combination fitting of the HERFD–XANES spectra for all samples using only U(VI) and U(IV) standards; however, this yielded unsatisfactory results (Figures S6 and S7, Table S3). The linear combination fits for all samples were improved using either a uranyl(V)^{30,69} or a uranate(V)^{70,71} standard with the U(IV) and U(VI) standards (Figures S6 and S7, Table S3). Our data confirmed U(V) as a major reaction product in the reduction of U(VI) by *S. oneidensis* MR1, although as fits using uranyl(V) only provided marginally better fits than uranate(V), the exact geometry of U(V) at 4.5 h remains inconclusive (Figure S7, Table S3). Linear combination fits for the 4.5 h cell suspension showed either 59% uranyl(V) or 36% uranate(V), with the remaining uranium present as uranyl(VI), consistent with luminescence data and literature.⁹ The 4.5 h cell pellet was fitted with either 71% uranyl(V) or 47% uranate(V) and 23–24% UO_2 , with the remaining uranium present as uranyl(VI). This suggests that U(V) can remain associated with the biomass during bioreduction/disproportionation. Interestingly, the U(IV) signal observed on solids was below the detection limit in the cell suspension due to different contributions from the

solution and the solid phase in these two samples (Figures 1 and 2, Table S3). For the 120.5 h sample, a cell pellet was

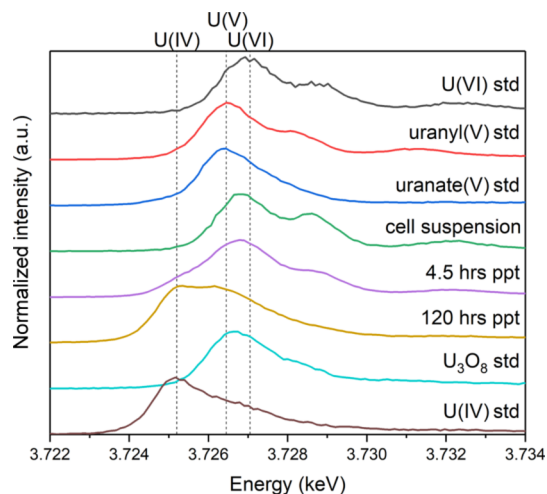


Figure 2. Normalized U M_4 -edge HERFD-XANES spectra for the solid phase: U(IV) O_2 standard (brown); U_3O_8 (2 U(V):1 U(VI)) standard (turquoise); 120.5 h end-point (yellow), 4.5 h cell precipitate (purple), 4.5 h cell suspension (green), uranate(V) standard (blue), uranyl(V) standard (red), and U(VI) O_3 standard (black) (std and ppt are used as abbreviations for standard and precipitate, respectively).

analyzed and the M_4 -edge HERFD-XANES showed clear differences to the chemically precipitated U(IV) O_2 standard. Here, linear combination fitting between U(VI), (V), and (IV) estimated approximately 26–28% U(V) and 72–74% U(IV)- O_2 was present in the sample for both uranyl(V) and uranate(V) fits, respectively (Figures S6 and S7, Table S3). Again, this suggests a significant fraction of U(V) in the cell pellet over 120.5 h (Figure S7, Table S3). Typically, the accuracy of oxidation state determination from XANES data is ± 10 –15%.⁷²

X-ray Absorption Spectroscopy: U L_3 -Edge. U L_3 -edge XANES and EXAFS data collected on cell suspensions from cultures of *S. oneidensis* MR1 supplied with uranyl(VI) were collected after 2.5 and 4.5 h, and on the cell pellet collected at 120.5 h. The edge position for the samples at 2.5 and 4.5 h

were in between the U(VI) and U(IV) standards, which suggested that the cell suspensions contained a mixture of U-oxidation states (Table S4, Figure S7). The structure is also different from the U(VI) and U(IV) standards, which may be due to the presence of other U species. By the 120.5 h end point, the U L_3 -edge XANES matched the U(IV) standard, suggesting that U(IV) dominated in the sample (Figure S6 and Table S3). Unlike U M_4 -edge HERFD-XANES, U L_3 -edge XANES cannot fully quantify the uranium oxidation state in complex samples with mixed U(VI), (V), and (IV) oxidation states.^{38,73} Specifically in the case of complex spectra of the type expected in these bioreduction experiments, quantifying U(VI), (V), and (IV) contributions with U L_3 -edge XANES is challenging.^{38,73}

Fitting of the U L_3 -edge EXAFS data was used to further explore the speciation of U and the distribution of U(VI), (V), and (IV) in the samples. Although EXAFS fitting does not provide direct information regarding the oxidation state, the fitting parameters obtained can be used to indirectly infer U-oxidation states. Here, the characteristic presence and extension of the uranyl $U=O_{ax}$ bond length from 1.8 Å for uranyl(VI) to 1.9 Å for uranyl(V),^{9,22,32,35} and the lack of a $U-O$, uranate(V), bond length at 2.1–2.2 Å^{40,44,74,75} were particularly pertinent in fitting. Any attempts of fitting using a uranate-like speciation proved unsuccessful. Overall the EXAFS and associated Fourier transforms for the 2.5 and 4.5 h cell suspension samples were remarkably consistent (Figure 3). Informed by the relevant literature, the 2.5 h cell suspension was fitted as uranyl triscarbonate species.^{9,10} Here, the best fit was consistent with an average $U=O_{ax}$ bond length of 1.86 Å (Table 1), supporting an approximately 40 \pm 10%:60 \pm 10% contribution from uranyl(VI) (1.8 Å^{9,32,35,76}) and uranyl(V) (1.9 Å^{9,32,35,76}). We note that this ratio should be treated as an estimate as it will be affected by the number of species and their relative Debye-Waller factors; although the Debye-Waller factors for both uranyl(V/VI) species have been shown to be very similar.^{32,35} Nonetheless, this suggests a significant reduction from the uranyl(VI) species in this sample. The dioxygenyl bond length is significantly longer than values for uranyl(VI) (1.79–1.80 Å^{32,35,76}), it is also significantly shorter than $U-O$ bond lengths in uranate(V/VI) complexes (2.11–2.18 and 2.36–2.42 Å for uranate(V/VI), respectively^{40,44,74,75}), suggesting a mixed valence, uranyl(V/VI)

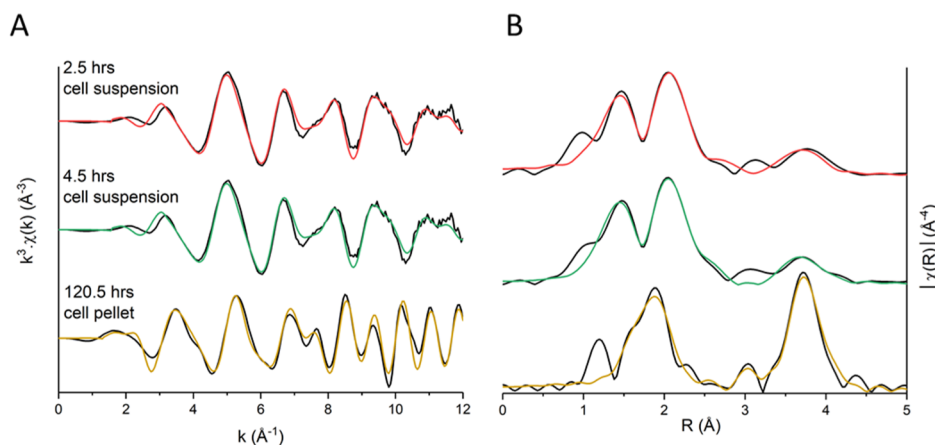


Figure 3. U L_3 -edge EXAFS spectra for uranyl(VI) reduced by *S. oneidensis* MR1 after 2.5 h (cell suspension) (red), 4.5 h (cell suspension) (green) and 120.5 h (precipitate, with uranyl(V) contribution) (yellow). Panel (A) k^3 -weighted EXAFS; panel (B) Fourier transform of k^3 -weighted EXAFS. Black lines show experimental data and colored lines show the fits described in Table 1.

Table 1. Fitting Parameters Obtained from U L₃-Edge EXAFS Spectroscopy^a

sample	scattering path	N	R (Å)	σ^2 (Å ²)	S ₀ ²	R-factor	α^b
2.5 h cell suspension	U=O _{ax}	2	1.86(1)	0.008(1)	1	0.014	99.9 ^c
	U–O _{eq}	4	2.37(3)	0.012(7)			
	U–O _{eq}	2	2.48(1)	0.004(1)			
	U...C	3	2.93(2)	0.003(2)			
	U...O _{dist}	3	4.22(2)	0.006(2)			
	(MS) U...O _{dist}	6	4.21(2)*	0.006(2)*			
4.5 h cell suspension	(MS) U...O _{dist}	3	4.21(2)*	0.006(2)*	1	0.016	100.0 ^c
	U=O _{ax}	2	1.86(1)	0.008(2)			
	U–O _{eq}	4	2.36(3)	0.010(6)			
	U–O _{eq}	2	2.49(1)	0.003(1)			
	U...C	3	2.92(2)	0.005(2)			
	U...O _{dist}	3	4.23(1)	0.007(2)			
120.5 h cell pellet with U(V)	(MS) U...O _{dist}	6	4.21(2)*	0.007(2)*	1	0.017	99.9 ^d
	(MS) U...O _{dist}	3	4.21(2)*	0.007(2)*			
	U=O _{ax}	0.4	1.92(5)	0.008(5)			
	U–O	7	2.36(0)	0.012(1)			
	U–U	12	3.86(1)	0.008(0)			
	U–O _{dist}	24	4.44(0)	0.009(1)			

^aN, R, σ^2 , S₀² and the R-factor refer to the coordination number, radial distance, Debye–Waller factor, amplitude correction factor, and the goodness of fit, respectively. Uncertainty in interatomic distances is quoted in brackets for the last decimal place (Å). Spectra have been plotted in R and k³ in Figure 3. * Parameters fixed during fitting. ^bF-test results; $\alpha > 0.95$ statistically improves the fit with 2 σ confidence.⁷⁷ ^cF-test results for adding the U–O_{dist} feature and associated multiple scatterers at 4.2 Å. ^dF-test results for adding the U(V)=O_{ax} feature at 1.9 Å.

system at 2.5 and 4.5 h. The equatorial shell was fitted as a split shell with 2 O backscatterers at approximately 2.4 Å (consistent with uranyl(VI) equatorial oxygen 2.42–2.45 Å^{9,32,35,76}) and four O backscatterers at approximately 2.5 Å (consistent with uranyl(V) equatorial oxygen 2.47–2.50 Å^{9,32,35}) (Table 1). Additional features in the EXAFS and Fourier transform were successfully modeled by inclusion of 3 C backscatterers at approximately 2.9 Å, and 3 O backscatterers at approximately 4.2 Å. Again, these are consistent with contributions from uranyl(VI) and uranyl(V) triscarbato species (U(VI, V)–C = 2.88–2.94 Å, and U(VI, V)–O_{dist} = 4.13–4.28 Å^{9,32,35,76}) and support significant reduction to uranyl(V) at 2.5 h. This is consistent with the luminescence data which showed significant reduction in uranyl(VI) luminescence at 2.5 h. For both the 2.5 and 4.5 h samples, the EXAFS and Fourier transform data were similar (Figure 3) and here, the 4.5 h sample could be fitted with essentially the same coordination environment as the 2.5 h sample (Table 1). The EXAFS fits for the data at 4.5 h were consistent with the 4.5 h U M₄-edge HERFD–XANES LCF analysis using a uranyl(V) standard showing approximately ~60% U(V), present as uranyl(V) (Figure 3). Interestingly, the geochemical data and U M₄-edge linear combination fitting results suggest that up to 10% U(IV) may be present at 4.5 h (Figures 1 and 2). A fit containing 10% U(IV) contribution improved the results, although the additional shell did not contribute statistically to the fit and was thus not included. Overall, EXAFS fitting for the 2.5 and 4.5 h cell suspensions showed evidence for the extension of the dioxygenyl bond length in uranyl(VI) (1.8 Å;^{9,32}) to 1.86 Å. These fits are consistent with approximately 40% uranyl(VI) and 60% uranyl(V) in the samples, which agreed with the luminescence data (Figure 1), the U M₄-edge HERFD–XANES LCF using a uranyl(V) standard (Figure 2), and with past work, where approximately 60% reduction to uranyl(V) was reported for bioreduction with *G. sulfurreducens* at 4 h.⁹ This suggested uranyl(V) as a transient bioreduction product in agreement with micro-

biological studies,^{9,10,12} and in contrast to recent work on U(V) stabilization in Fe-oxides where uranate(V)-like incorporation dominates.^{40,44}

Finally, the 120.5 h cell pellet EXAFS data were first fitted with 8 O backscatterers at 2.36 Å and 12 U backscatterers at 3.86 Å, consistent with crystalline uraninite and in agreement with past work.^{51,52} However, because of unsatisfactory σ^2 values in the U–O scattering paths (Table S2), and with the new information suggesting a U(V) state in the end-point, we further considered a contribution from U(V) in the U L₃-edge EXAFS fitting for the end-point sample again informed by the relevant literature.^{9,32} The Fourier transform showed a feature at ~1.9 Å before the U(IV)–O shell in uraninite at 2.36 Å. Here, we attempted a fit with approximately 20% of uranyl(V), which statistically contributed to the fit (F-test 99.9%). The resulting fit with a modest 0.4 axial U=O_{ax} backscattering contribution at 1.92 Å and with a reduced U–O contribution of 7 O was consistent with an approximately 20% contribution from uranyl(V) in the bioreduction end point (Tables 1, S4 and Figure 3). This estimate is consistent with the linear combination fitting value of approximately 28% uranyl(V) estimated with U M₄-edge HERFD–XANES. Our interpretation of these data suggests, for the first time, the presence of a long-lived 20–30% uranyl(V) intermediate associated with the biomass/precipitate after 5-days of bioreduction.

Where most work on U(V) under environmentally relevant conditions has addressed the role of Fe in stabilizing U(V),^{40,41,44,78} the combined approach presented here increases the understanding and importance of U(V) in biological systems by demonstrating that *S. oneidensis* MRI operates a one electron transfer mechanism for uranyl(VI) bioreduction. In the supernatant, the difference in total U_(aq), as determined by ICPMS, and the uranyl(VI) concentrations, as determined by luminescence spectroscopy, suggested that up to ~60% of the U was present as a nonuranyl(VI) species in solution at 2.5 and 4.5 h. Here, further analysis of cell suspensions, where the U signal is dominated by aqueous U,

using U M_4 -edge HERFD–XANES defined a significant portion of the species as pentavalent U; although it was not possible to distinguish between uranyl(V) and uranate(V)-like speciation. In the U L_3 -edge EXAFS, the characteristic extension of the U=O_{ax} bond and the lack of a uranate U–O bond are consistent with uranyl(V) after 2.5 and 4.5 h of bioreduction, although this requires further investigation. In agreement with previous findings, this work suggests that biological uranyl(VI) reduction pathways preferentially reduce via 1 electron transfer mechanisms. Given that *S. oneidensis* MR1 reduces U(VI) via the Mtr extracellular pathway which transfers one electron at a time, the results published here are consistent with relevant literature.^{13,14,79,80} Also, this is similar to the single electron transfer mechanisms observed in U(VI) reduction pathways in iron-rich geological systems.^{40,44} The presence of U(V) in both the cell suspension and the cell precipitate suggests that the U(V) was not associated exclusively with the cells, in agreement with similar *Geobacter* systems.^{9,10} This suggests that the mechanism(s) of electron transfer from *S. oneidensis* MR1 to U(VI) could involve multiple (intracellular and extracellular) electron transfer pathways, as supported by the relevant literature.^{13–16,81} Furthermore, we have established that U(V) can persist for appreciable lifetimes (at least 120.5 h) under environmentally relevant conditions in contrast to past studies, where it has been considered transient (less than 24 h).^{9,10} The discovery of a potentially persistent U(V) species in the endpoint sample suggests that it could play a previously unrecognized role in the remobilization of “bioreduced” U. In turn, this greatly improves the mechanistic understanding of environmental U speciation and it further broadens the field of stability for U(V) at circumneutral pH. Indeed, U(V) behavior in environmental conditions has not yet been fully explored, and thus further work in more environmentally relevant settings are merited.

■ ASSOCIATED CONTENT

Supporting Information

The Supporting Information is available free of charge at <https://pubs.acs.org/doi/10.1021/acs.est.9b05285>.

Additional information on U sorption to autoclaved cells, aqueous and luminescence analyses and X-ray absorption spectroscopy: (U L_3 -edge XANES; U L_3 -edge EXAFS; and, M_4 -edge HERFD–XANES) (PDF)

■ AUTHOR INFORMATION

Corresponding Author

Jonathan R. Lloyd – Williamson Research Centre for Molecular Environmental Science and Research Centre for Radwaste Disposal, Department of Earth and Environmental Science, School of Natural Sciences, The University of Manchester, Manchester M13 9PL, England; Email: jon.lloyd@manchester.ac.uk

Authors

Gianni F. Vettese – Williamson Research Centre for Molecular Environmental Science and Research Centre for Radwaste Disposal, Department of Earth and Environmental Science, School of Natural Sciences, The University of Manchester, Manchester M13 9PL, England; orcid.org/0000-0003-0510-9542

Katherine Morris – Williamson Research Centre for Molecular Environmental Science and Research Centre for Radwaste

Disposal, Department of Earth and Environmental Science, School of Natural Sciences, The University of Manchester, Manchester M13 9PL, England; orcid.org/0000-0002-0716-7589

Louise S. Natrajan – Centre for Radiochemistry Research, Department of Chemistry, School of Natural Sciences, The University of Manchester, Manchester M13 9PL, England; orcid.org/0000-0002-9451-3557

Samuel Shaw – Williamson Research Centre for Molecular Environmental Science and Research Centre for Radwaste Disposal, Department of Earth and Environmental Science, School of Natural Sciences, The University of Manchester, Manchester M13 9PL, England; orcid.org/0000-0002-6353-5454

Tonya Vitova – Institute for Nuclear Waste Disposal (INE), Karlsruhe Institute of Technology, Karlsruhe 76131, Germany; orcid.org/0000-0002-3117-7701

Jurij Galanzew – Institute for Nuclear Waste Disposal (INE), Karlsruhe Institute of Technology, Karlsruhe 76131, Germany

Debbie L. Jones – College of Environmental Sciences and Engineering, Bangor University, Bangor LL57 2DG, U.K.

Complete contact information is available at: <https://pubs.acs.org/10.1021/acs.est.9b05285>

Author Contributions

The manuscript was written through contributions of all authors. All the authors have given approval to the final version of the manuscript.

Notes

The authors declare no competing financial interest.

■ ACKNOWLEDGMENTS

This work was funded by the Nuclear Decommissioning Authority (NDA) managed by the National Nuclear Laboratory (NNL). We also acknowledge funding from the NERC funded OPTIUM (Optical Imaging of Uranium Biotransformations by Microorganisms) grant (NE/R011230/1), Diamond Light Source (DLS) for beamtime awards (SP17243 and SP13559), and the KIT synchrotron radiation source for beamtime access. The KIT Institute for Beam Physics and Technology (IBPT) is acknowledged for the operation of the storage ring, the Karlsruhe Research Accelerator (KARA), and provision of beamtime at the KIT synchrotron source. We thank Steven Parry and Giannantonio Cibir for beamtime assistance at DLS and Bianca Schacherl at the KIT synchrotron radiation source. We also thank Luke Townsend, Kurt Smith, and Thomas Neill for assistance with data analysis, Paul Lythgoe for data acquisition, and Pieter Bots and Thomas Neill for the XAS spectra of synthetic UO₂ and [UO₂(CO₃)₃]⁴⁻, respectively.

■ REFERENCES

- (1) Lovley, D. R.; Phillips, E. J. P.; Gorby, Y. a.; Landa, E. R. Microbial Reduction of Uranium. *Nature* **1991**, *350*, 413–416.
- (2) Anderson, R. T.; Vrionis, H. A.; Ortiz-Bernad, I.; Resch, C. T.; Long, P. E.; Dayvault, R.; Karp, K.; Marutzky, S.; Metzler, D. R.; Peacock, A.; White, D. C.; Lowe, M.; Lovley, D. R. Stimulating the In Situ Activity of *Geobacter* Species to Remove Uranium from the Groundwater of a Uranium-Contaminated Aquifer. *Appl. Environ. Microbiol.* **2003**, *69*, S884–S891.
- (3) Williams, K. H.; Long, P. E.; Davis, J. a.; Wilkins, M. J.; N'Guessan, a. L.; Steefel, C. I.; Yang, L.; Newcomer, D.; Spane, F. a.; Kerkhof, L. J.; McGuinness, L.; Dayvault, R.; Lovley, D. R. Acetate

Availability and Its Influence on Sustainable Bioremediation of Uranium-Contaminated Groundwater. *Geomicrobiol. J.* **2011**, *28*, 519–539.

(4) Yabusaki, S. B.; Fang, Y.; Long, P. E.; Resch, C. T.; Peacock, A. D.; Komlos, J.; Jaffe, P. R.; Morrison, S. J.; Dayvault, R. D.; White, D. C.; Anderson, R. T. Uranium Removal from Groundwater via in Situ Biostimulation: Field-Scale Modeling of Transport and Biological Processes. *J. Contam. Hydrol.* **2007**, *93*, 216–235.

(5) Williams, K. H.; Bargar, J. R.; Lloyd, J. R.; Lovley, D. R. Bioremediation of Uranium-Contaminated Groundwater: A Systems Approach to Subsurface Biogeochemistry. *Curr. Opin. Biotechnol.* **2013**, *24*, 489–497.

(6) Newsome, L.; Morris, K.; Lloyd, J. R. The Biogeochemistry and Bioremediation of Uranium and Other Priority Radionuclides. *Chem. Geol.* **2014**, *363*, 164–184.

(7) Reguera, G.; McCarthy, K. D.; Mehta, T.; Nicoll, J. S.; Tuominen, M. T.; Lovley, D. R. Extracellular Electron Transfer via Microbial Nanowires. *Nature* **2005**, *435*, 1098–1101.

(8) Shi, L.; Richardson, D. J.; Wang, Z.; Kerisit, S. N.; Rosso, K. M.; Zachara, J. M.; Fredrickson, J. K. The Roles of Outer Membrane Cytochromes of *Shewanella* and *Geobacter* in Extracellular Electron Transfer. *Environ. Microbiol. Rep.* **2009**, *1*, 220–227.

(9) Renshaw, J. C.; Butchins, L. J. C.; Livens, F. R.; May, I.; Charnock, J. M.; Lloyd, J. R. Bioreduction of Uranium: Environmental Implications of a Pentavalent Intermediate. *Environ. Sci. Technol.* **2005**, *39*, 5657–5660.

(10) Jones, D. L.; Andrews, M. B.; Swinburne, A. N.; Botchway, S. W.; Ward, A. D.; Lloyd, J. R.; Natrajan, L. S. Fluorescence Spectroscopy and Microscopy as Tools for Monitoring Redox Transformations of Uranium in Biological Systems. *Chem. Sci.* **2015**, *6*, 5133–5138.

(11) Sundararajan, M.; Campbell, A. J.; Hillier, I. H. Catalytic Cycles for the Reduction of [UO₂]²⁺ by Cytochrome c7 Proteins Proposed from DFT Calculations. *J. Phys. Chem. A* **2008**, *112*, 4451–4457.

(12) Großmann, K.; Arnold, T.; Krawczyk-Bärsch, E.; Diessner, S.; Wobus, A.; Bernhard, G.; Krawietz, R. Identification of Fluorescent U(V) and U(VI) Microparticles in a Multispecies Biofilm by Confocal Laser Scanning Microscopy and Fluorescence Spectroscopy. *Environ. Sci. Technol.* **2007**, *41*, 6498–6504.

(13) Marshall, M. J.; Beliaev, A. S.; Dohnalkova, A. C.; Kennedy, D. W.; Shi, L.; Wang, Z.; Boyanov, M. I.; Lai, B.; Kemner, K. M.; McLean, J. S.; Reed, S. B.; Culley, D. E.; Bailey, V. L.; Simonson, C. J.; Saffarini, D. A.; Romine, M. F.; Zachara, J. M.; Fredrickson, J. K. C-Type Cytochrome-Dependent Formation of U(IV) Nanoparticles by *Shewanella Oneidensis*. *PLoS Biol.* **2006**, *4*, No. e268.

(14) Cherkouk, A.; Law, G. T. W.; Rizoulis, A.; Law, K.; Renshaw, J. C.; Morris, K.; Livens, F. R.; Lloyd, J. R. Influence of Riboflavin on the Reduction of Radionuclides by *Shewanella Oneidensis* MR-1. *Dalton Trans.* **2016**, *45*, 5030–5037.

(15) Suzuki, Y.; Kitatsuji, Y.; Ohnuki, T.; Tsujimura, S. Flavin Mononucleotide Mediated Electron Pathway for Microbial U(VI) Reduction. *Phys. Chem. Chem. Phys.* **2010**, *12*, 10081–10087.

(16) Kotloski, N. J.; Gralnick, J. A. Flavin Electron Shuttles Dominate Extracellular Electron Transfer by *Shewanella Oneidensis*. *mBio* **2013**, *4*, No. e00553.

(17) Orlandini, K. A.; Penrose, W. R.; Nelson, D. M. Pu(V) as the Stable Form of Oxidized Plutonium in Natural Waters. *Mar. Chem.* **1986**, *18*, 49–57.

(18) Nelson, D. M.; Lovett, M. B. Oxidation State of Plutonium in the Irish Sea. *Nature* **1978**, *276*, 599–601.

(19) Kvashnina, K. O.; Romanchuk, A.; Pidchenko, I.; Amidani, L.; Gerber, E.; Trigub, A.; Rossberg, A.; Weiss, S.; Popa, K.; Walter, O.; Caciuffo, R.; Scheinost, A.; Butorin, S.; Kalmykov, S. A Novel Meta-Stable Pentavalent Plutonium Solid Phase on the Pathway from Aqueous Pu(VI) to PuO₂ Nanoparticles. *Angew. Chem., Int. Ed.* **2019**, *58*, 17558.

(20) Choppin, G. R.; Wong, P. J. The Chemistry of Actinide Behavior in Marine Systems. *Aquat. Geochem.* **1998**, *4*, 77–101.

(21) Runde, W. *The Chemical Interactions of Actinides in the Environment*; Los Alamos Science, 2000; pp 392–411.

(22) Arnold, P. L.; Love, J. B.; Patel, D. Pentavalent Uranyl Complexes. *Coord. Chem. Rev.* **2009**, *253*, 1973–1978.

(23) Berthet, J.-C.; Nierlich, M.; Ephritikhine, M. Isolation of a Uranyl [UO₂]⁺ Species: Crystallographic Comparison of the Dioxouranium(V) and (VI) Compounds [UO₂(OPPH₃)₄](OTf)_n (n = 1, 2). *Angew. Chem., Int. Ed.* **2003**, *42*, 1952–1954.

(24) Natrajan, L.; Burdet, F.; Pécaut, J.; Mazzanti, M. Synthesis and Structure of a Stable Pentavalent-Uranyl Coordination Polymer. *J. Am. Chem. Soc.* **2006**, *128*, 7152–7153.

(25) Hayton, T. W.; Wu, G. Synthesis, Characterization, and Reactivity of a Uranyl β -Diketimate Complex. *J. Am. Chem. Soc.* **2008**, *130*, 2005–2014.

(26) Hayton, T. W.; Wu, G. Mixed-Ligand Uranyl(V) β -Diketimate/ β -Diketone Complexes: Synthesis and Characterization. *Inorg. Chem.* **2008**, *47*, 7415–7423.

(27) Nocton, G.; Horeglad, P.; Vetere, V.; Pécaut, J.; Dubois, L.; Maldivi, P.; Edelstein, N. M.; Mazzanti, M. Synthesis, Structure, and Bonding of Stable Complexes of Pentavalent Uranyl. *J. Am. Chem. Soc.* **2010**, *132*, 495–508.

(28) Hayton, T. W.; Wu, G. Exploring the Effects of Reduction or Lewis Acid Coordination on the U=O Bond of the Uranyl Moiety. *Inorg. Chem.* **2009**, *48*, 3065–3072.

(29) Schettini, M. F.; Wu, G.; Hayton, T. W. Coordination of N-Donor Ligands to a Uranyl(V) β -Diketimate Complex. *Inorg. Chem.* **2009**, *48*, 11799–11808.

(30) Zegke, M.; Zhang, X.; Pidchenko, I.; Hlina, J. A.; Lord, R. M.; Purkis, J.; Nichol, G. S.; Magnani, N.; Schreckenbach, G.; Vitova, T.; Love, J. B.; Arnold, P. L. Differential Uranyl(v) Oxo-Group Bonding between the Uranium and Metal Cations from Groups 1, 2, 4, and 12; A High Energy Resolution X-Ray Absorption, Computational, and Synthetic Study. *Chem. Sci.* **2019**, *10*, 9740–9751.

(31) Wester, D. W.; Sullivan, J. C. Electrochemical and Spectroscopic Studies of Uranium(IV), -(V), and -(VI) in Carbonate-Bicarbonate Buffers. *Inorg. Chem.* **1980**, *19*, 2838–2840.

(32) Docrat, T. I.; Mosselmans, J. F. W.; Charnock, J. M.; Whiteley, M. W.; Collison, D.; Livens, F. R.; Jones, C.; Edmiston, M. J. X-Ray Absorption Spectroscopy of Tricarbonatodioxouranate(V), [UO₂(CO₃)₃]⁵⁻, in Aqueous Solution. *Inorg. Chem.* **1999**, *38*, 1879–1882.

(33) Cohen, D. The Preparation and Spectrum of Uranium(V) Ions in Aqueous Solutions. *J. Inorg. Nucl. Chem.* **1970**, *32*, 3525–3530.

(34) Madic, C.; Hobart, D. E.; Begun, G. M. Raman Spectrometric Studies of Actinide(V) and (VI) Complexes in Aqueous Sodium Carbonate Solution and of Solid Sodium Actinide(V) Carbonate Compounds. *Inorg. Chem.* **1983**, *22*, 1494–1503.

(35) Ikeda, A.; Hennig, C.; Tsushima, S.; Takao, K.; Ikeda, Y.; Scheinost, A. C.; Bernhard, G. Comparative Study of Uranyl(VI) and -(V) Carbonate Complexes in an Aqueous Solution. *Inorg. Chem.* **2007**, *46*, 4212–4219.

(36) Mizuoka, K.; Grenthe, I.; Ikeda, Y. Structural and Kinetic Studies on Uranyl(V) Carbonate Complex Using ¹³C NMR Spectroscopy. *Inorg. Chem.* **2005**, *44*, 4472–4474.

(37) Faizova, R.; Scopelliti, R.; Chauvin, A.-S.; Mazzanti, M. Synthesis and Characterization of a Water Stable Uranyl(V) Complex. *J. Am. Chem. Soc.* **2018**, *140*, 13554–13557.

(38) Kvashnina, K. O.; Butorin, S. M.; Martin, P.; Glatzel, P. Chemical State of Complex Uranium Oxides. *Phys. Rev. Lett.* **2013**, *111* (). <https://doi.org/10.1103/PhysRevLett.111.253002>. DOI: 10.1103/physrevlett.111.253002

(39) Burns, P. C.; Finch, R. J. Wyratite; crystallographic evidence for the first pentavalent-uranium mineral. *Am. Mineral.* **1999**, *84*, 1456–1460.

(40) Roberts, H. E.; Morris, K.; Law, G. T. W.; Mosselmans, J. F. W.; Bots, P.; Kvashnina, K.; Shaw, S. Uranium(V) Incorporation Mechanisms and Stability in Fe(II)/Fe(III) (Oxyhydr)Oxides. *Environ. Sci. Technol. Lett.* **2017**, *4*, 421–426.

- (41) Collins, R. N.; Rosso, K. M. Mechanisms and Rates of U(VI) Reduction by Fe(II) in Homogeneous Aqueous Solution and the Role of U(V) Disproportionation. *J. Phys. Chem. A* **2017**, *121*, 6603–6613.
- (42) Tsarev, S.; Collins, R. N.; Fahy, A.; Waite, T. D. Reduced Uranium Phases Produced from Anaerobic Reaction with Nanoscale Zerovalent Iron. *Environ. Sci. Technol.* **2016**, *50*, 2595–2601.
- (43) Sun, Y.; Lan, J.; Li, M.; Hu, W.; Liu, H.; Song, G.; Chen, D.; Shi, W.; Wang, X. Influence of Aqueous Sulfide on Speciation of U(VI) Adsorbed to Nanomagnetite. *Environ. Sci.: Nano* **2018**, *5*, 1981–1989.
- (44) Pidchenko, I.; Kvashnina, K. O.; Yokosawa, T.; Finck, N.; Bahl, S.; Schild, D.; Polly, R.; Bohner, E.; Rossberg, A.; Göttlicher, J.; Dardenne, K.; Rothe, J.; Schäfer, T.; Geckeis, H.; Vitova, T. Uranium Redox Transformations after U(VI) Coprecipitation with Magnetite Nanoparticles. *Environ. Sci. Technol.* **2017**, *51*, 2217–2225.
- (45) Kerisit, S.; Bylaska, E. J.; Massey, M. S.; McBriarty, M. E.; Ilton, E. S. Ab Initio Molecular Dynamics of Uranium Incorporated in Goethite (α -FeOOH): Interpretation of X-Ray Absorption Spectroscopy of Trace Polyvalent Metals. *Inorg. Chem.* **2016**, *55*, 11736–11746.
- (46) Tsarev, S.; Collins, R. N.; Ilton, E. S.; Fahy, A.; Waite, T. D. The Short-Term Reduction of Uranium by Nanoscale Zero-Valent Iron (NZVI): Role of Oxide Shell, Reduction Mechanism and the Formation of U(V)-Carbonate Phases. *Environ. Sci.: Nano* **2017**, *4*, 1304–1313.
- (47) Ilton, E. S.; Bagus, P. S. XPS Determination of Uranium Oxidation States. *Surf. Interface Anal.* **2011**, *43*, 1549–1560.
- (48) Marshall, T. A.; Morris, K.; Law, G. T. W.; Frederick, J.; Bots, P.; Roberts, H.; Shaw, S. Uranium Fate during Crystallization of Magnetite from Ferrihydrite in Conditions Relevant to the Disposal of Radioactive Waste. *Mineral. Mag.* **2015**, *79*, 1265–1274.
- (49) Vitova, T.; Denecke, M. A.; Göttlicher, J.; Jorissen, K.; Kas, J. J.; Kvashnina, K.; Prüfmann, T.; Rehr, J. J.; Rothe, J. Actinide and Lanthanide Speciation with High-Energy Resolution X-Ray Techniques. *J. Phys.: Conf. Ser.* **2013**, *430*, 012117.
- (50) Vitova, T.; Pidchenko, I.; Fellhauer, D.; Bagus, P. S.; Joly, Y.; Pruessmann, T.; Bahl, S.; Gonzalez-Robles, E.; Rothe, J.; Altmayer, M.; Denecke, M. A.; Geckeis, H. The Role of the 5f Valence Orbitals of Early Actinides in Chemical Bonding. *Nat. Commun.* **2017**, *8*, 16053.
- (51) Schofield, E. J.; Veeramani, H.; Sharp, J. O.; Suvorova, E.; Bernier-Latmani, R.; Mehta, A.; Stahlman, J.; Webb, S. M.; Clark, D. L.; Conradson, S. D.; Ilton, E. S.; Bargar, J. R. Structure of Biogenic Uraninite Produced by *Shewanella Oneidensis* Strain MR-1. *Environ. Sci. Technol.* **2008**, *42*, 7898–7904.
- (52) Bernier-Latmani, R.; Veeramani, H.; Vecchia, E. D.; Junier, P.; Lezama-Pacheco, J. S.; Suvorova, E. I.; Sharp, J. O.; Wigginton, N. S.; Bargar, J. R. Non-Uraninite Products of Microbial U(VI) Reduction. *Environ. Sci. Technol.* **2010**, *44*, 9456–9462.
- (53) Myers, C. R.; Nealson, K. H. Bacterial Manganese Reduction and Growth with Manganese Oxide as the Sole Electron Acceptor. *Science* **1988**, *240*, 1319–1321.
- (54) Zimina, A.; Dardenne, K.; Denecke, M. A.; Grunwaldt, J. D.; Huttel, E.; Lichtenberg, H.; Mangold, S.; Pruessmann, T.; Rothe, J.; Steininger, R.; Vitova, T. The CAT-ACT Beamline at ANKA: A New High Energy X-Ray Spectroscopy Facility for CATalysis and ACTinide Research. *J. Phys.: Conf. Ser.* **2016**, *712*, 012019.
- (55) Zimina, A.; Dardenne, K.; Denecke, M. A.; Doronkin, D. E.; Huttel, E.; Lichtenberg, H.; Mangold, S.; Pruessmann, T.; Rothe, J.; Spangenberg, T.; Steininger, R.; Vitova, T.; Geckeis, H.; Grunwaldt, J.-D. CAT-ACT - A New Highly Versatile x-Ray Spectroscopy Beamline for Catalysis and Radionuclide Science at the KIT Synchrotron Light Facility ANKA. *Rev. Sci. Instrum.* **2017**, *88*, 113113.
- (56) Ravel, B.; Newville, M. ATHENA, ARTEMIS, HEPHAESTUS: data analysis for X-ray absorption spectroscopy using IFEFFIT. *J. Synchrotron Radiat.* **2005**, *12*, 537–541.
- (57) Dent, A. J.; Cibin, G.; Ramos, S.; Smith, A. D.; Scott, S. M.; Varandas, L.; Pearson, M. R.; Krumpa, N. A.; Jones, C. P.; Robbins, P. E. B18: A Core XAS Spectroscopy Beamline for Diamond. *J. Phys.: Conf. Ser.* **2009**, *190*, 012039.
- (58) Parkhurst, D. L.; Appelo, C. A. J. *PHREEQC (Version 3)-A Computer Program for Speciation, Batch-Reaction, One-Dimensional Transport, and Inverse Geochemical Calculations*, 2013. <https://doi.org/Rep.99-4259>.
- (59) Watanabe, T.; Ikeda, Y. A Study on Identification of Uranyl Complexes in Aqueous Solutions Containing Carbonate Ion and Hydrogen Peroxide. *Energy Procedia* **2013**, *39*, 81–95.
- (60) Wang, Z.; Zachara, J. M.; Liu, C.; Gassman, P. L.; Felmy, A. R.; Clark, S. B. A Cryogenic Fluorescence Spectroscopic Study of Uranyl Carbonate, Phosphate and Oxyhydroxide Minerals. *Radiochim. Acta* **2008**, *96*, 591–598.
- (61) Natrajan, L. S. Developments in the Photophysics and Photochemistry of Actinide Ions and Their Coordination Compounds. *Coord. Chem. Rev.* **2012**, *256*, 1583–1603.
- (62) Grossmann, K.; Arnold, T.; Ikeda-Ohno, A.; Steudtner, R.; Geipel, G.; Bernhard, G. Fluorescence Properties of a Uranyl(V)-Carbonate Species [U(V)O₂(CO₃)₃]⁵⁻ at Low Temperature. *Spectrochim. Acta A Mol. Biomol. Spectrosc.* **2009**, *72*, 449–453.
- (63) Kirishima, A.; Kimura, T.; Tochiyama, O.; Yoshida, Z. Luminescence Study of Tetravalent Uranium in Aqueous Solution. *Chem. Commun.* **2003**, *3*, 910–911.
- (64) Ekstrom, A. Kinetics and Mechanism of the Disproportionation of Uranium(V). *Inorg. Chem.* **1974**, *13*, 2237–2241.
- (65) Newsome, L.; Morris, K.; Shaw, S.; Trivedi, D.; Lloyd, J. R. The Stability of Microbially Reduced U(IV); Impact of Residual Electron Donor and Sediment Ageing. *Chem. Geol.* **2015**, *409*, 125–135.
- (66) Moon, H. S.; Komlos, J.; Jaffé, P. R. Biogenic U(IV) Oxidation by Dissolved Oxygen and Nitrate in Sediment after Prolonged U(VI)/Fe(III)/SO₄²⁻ Reduction. *J. Contam. Hydrol.* **2009**, *105*, 18–27.
- (67) Moon, H. S.; Komlos, J.; Jaffé, P. R. Uranium Reoxidation in Previously Bioreduced Sediment by Dissolved Oxygen and Nitrate. *Environ. Sci. Technol.* **2007**, *41*, 4587–4592.
- (68) Sanyal, K.; Khooha, A.; Das, G.; Tiwari, M. K.; Misra, N. L. Direct Determination of Oxidation States of Uranium in Mixed-Valent Uranium Oxides Using Total Reflection X-Ray Fluorescence X-Ray Absorption Near-Edge Spectroscopy. *Anal. Chem.* **2017**, *89*, 871–876.
- (69) Reta, D.; Ortu, F.; Randall, S.; Mills, D. P.; Chilton, N. F.; Wippeny, R. E. P.; Natrajan, L.; Edwards, B.; Kaltsoyannis, N. The Performance of Density Functional Theory for the Description of Ground and Excited State Properties of Inorganic and Organometallic Uranium Compounds. *J. Organomet. Chem.* **2018**, *857*, 58–74.
- (70) Randall, S. *Preparation and Investigation into the Optical Properties of Air Sensitive f-Block Complexes*; The University of Manchester, 2015.
- (71) Popa, K.; Prieur, D.; Manara, D.; Naji, M.; Vigier, J.-F.; Martin, P. M.; Dieste Blanco, O.; Scheinost, A. C.; Prüfmann, T.; Vitova, T.; Raison, P. E.; Somers, J.; Konings, R. J. M. Further Insights into the Chemistry of the Bi-U-O System. *Dalton Trans.* **2016**, *45*, 7847–7855.
- (72) Boyanov, M. I.; O'Loughlin, E. J.; Roden, E. E.; Fein, J. B.; Kemner, K. M. Adsorption of Fe(II) and U(VI) to Carboxyl-Functionalized Microspheres: The Influence of Speciation on Uranyl Reduction Studied by Titration and XAFS. *Geochim. Cosmochim. Acta* **2007**, *71*, 1898–1912.
- (73) Bès, R.; Rivenet, M.; Solari, P.-L.; Kvashnina, K. O.; Scheinost, A. C.; Martin, P. M. Use of HERFD-XANES at the U L₃- and M₄-Edges to Determine the Uranium Valence State on [Ni(H₂O)₄]₃[U(OH₂)(UO₂)₈O₁₂(OH)₃]. *Inorg. Chem.* **2016**, *55*, 4260–4270.
- (74) Soldatov, A. V.; Lamoén, D.; Konstantinović, M. J.; Van den Bergh, S.; Scheinost, A. C.; Verwerf, M. Local Structure and Oxidation State of Uranium in Some Ternary Oxides: X-Ray Absorption Analysis. *J. Solid State Chem.* **2007**, *180*, 54–61.
- (75) Kemmler, S. Zur Kristallstruktur von LiUO₃. *Z. Anorg. Allg. Chem.* **1965**, *338*, 9–14.
- (76) Catalano, J. G.; Brown, G. E. Analysis of Uranyl-Bearing Phases by EXAFS Spectroscopy: Interferences, Multiple Scattering, Accuracy

of Structural Parameters, and Spectral Differences. *Am. Mineral.* **2004**, *89*, 1004–1021.

(77) Downward, L.; Booth, C. H.; Lukens, W. W.; Bridges, F.; Division, C. S.; Berkeley, L. A Variation of the F- Test for Determining Statistical Relevance of Particular Parameters in EXAFS Fits. *X-Ray Absorption Fine Structure—XAFS13 13th International Conference*, 2007; Vol. 882, pp 2–4.

(78) Ilton, E. S.; Haiduc, A.; Cahill, C. L.; Felmy, A. R. Mica Surfaces Stabilize Pentavalent Uranium. *Inorg. Chem.* **2005**, *44*, 2986–2988.

(79) Coursolle, D.; Baron, D. B.; Bond, D. R.; Gralnick, J. A. The Mtr Respiratory Pathway Is Essential for Reducing Flavins and Electrodes in *Shewanella Oneidensis*. *J. Bacteriol.* **2010**, *192*, 467–474.

(80) Shi, L.; Rosso, K. M.; Zachara, J. M.; Fredrickson, J. K. Mtr Extracellular Electron-Transfer Pathways in Fe(III)-Reducing or Fe(II)-Oxidizing Bacteria: A Genomic Perspective. *Biochem. Soc. Trans.* **2012**, *40*, 1261–1267.

(81) Von Canstein, H.; Ogawa, J.; Shimizu, S.; Lloyd, J. R. Secretion of Flavins by *Shewanella* Species and Their Role in Extracellular Electron Transfer. *Appl. Environ. Microbiol.* **2008**, *74*, 615–623.